Geophys. J. Int. (1996) **126**, 437–446

Improved methods for solving for the magnetic field in E-polarization induction problems with fixed and staggered grids

J. T. Weaver, X. H. Pu* and A. K. Agarwal

Department of Physics and Astronomy and School of Earth and Ocean Sciences, University of Victoria, Victoria, BC, Canada, V8W 3P6

Accepted 1996 March 19. Received 1996 March 11; in original form 1995 September 14

SUMMARY

Solving by finite differences for the magnetic field in an E-polarization induction problem is an unorthodox approach because it is simpler to obtain the solution for the single component of the electric field, from which the two magnetic components are readily found by differentiation. Nevertheless, when the E-polarization model appears as the 2-D limit on the boundary of some general 3-D problem in which a finite-difference method is being used to solve for the magnetic field, then the unorthodox approach arises quite naturally. In a previous paper on this subject, it was shown that this problem is beset with numerical difficulties, and a 9-point formula which incorporated the divergence-free nature of the magnetic field was proposed as a way of eliminating numerical instabilities and improving the accuracy of calculation for certain extreme models. For others, however, namely those with very high conductivity contrasts near the surface, it has since been found that even the 9-point formulae are not very accurate. Here we report on further improvements to the finite-difference formulae which lead to accurate results for these types of models while still preserving all the advantages offered by the previous modifications. Two methods are described and compared. In the first, a standard fixed grid is used and new 9-point formulae are derived which give both magnetic field components at each node, and a simpler and more effective finite-difference equation is obtained for one of the surface boundary conditions. In the other approach, a staggered grid is used in which the electric and two magnetic components each have their own grid points. Methods are also developed for calculating the surface electric field from the magnetic field solutions obtained on both types of grid. Calculations are performed for two different models which represent the types of configurations that have caused numerical problems in the past. It is found that both approaches give excellent results when compared with those generated by standard 2-D finite-difference programs which solve directly for the electric field, and since the numerical problems overcome are similar to those found in a general 3-D induction problem, it is concluded that fixed grids could also be used in three dimensions with an accuracy comparable to that provided by staggered grids.

Key words: Earth conductivity, electromagnetic induction, finite-difference methods, numerical techniques, staggered grid.

1 INTRODUCTION

This is a sequel to an earlier paper (Pu *et al.* 1993), hereafter referred to as P-A-W, in which we discussed some problems encountered in the numerical solution of E-polarization problems in geo-electromagnetic induction when the two magnetic components are used as the unknown field components. Normally, of course, such problems are solved in terms of the electric field parallel to the strike of the conductivity anomaly within the Earth, since this single field component acts like a scalar potential, i.e. the other (magnetic) field components can be derived from it by differentiation. When the 2-D configuration is on the side boundary of a 3-D grid, however, and when the full 3-D problem is being solved in terms of the magnetic field, then the solution of an E-polarization problem in terms of the two magnetic components emerges quite naturally on the boundary as the limiting case of the 3-D

* Now at: Institute of Geology, State Seismological Bureau, Beijing 100029, P. R. China.

equations. It would be possible, of course, to use as boundary values the magnetic components obtained by numerical differentiation from a separate calculation of the electric field by standard methods, but this procedure would be somewhat more complicated and less compatible with the general 3-D equations. Moreover, the numerical difficulties arising in the unconventional 2-D solution are similar to those inherent in 3-D methods, so the relatively simple and computationally less demanding numerical investigations in two dimensions which are the subject of this paper can provide useful information on the approach to be taken when solving 3-D induction problems.

In P-A-W we explained that, while the standard 5-point finite-difference formulations of the differential equations satisfied by the two magnetic field components could normally be solved with acceptable accuracy in the usual manner, for certain types of models such as that shown in Fig. 1(b) the results were problematic in that they differed from the standard solutions obtained by solving for the electric field by as much as 50 per cent at some critical points. Alternative formulations of the finite-difference equations were obtained by integrating the induction equation over each cell in the numerical grid, but these were found to be numerically unstable. The instability was overcome by incorporating an additional term involving the vanishing divergence of the magnetic field in the integrand, and using the resulting 9-point finite-difference formulae to solve for the magnetic field components. Not only were these equations numerically stable, but they also gave solutions for models of the type shown in Fig. 1(b) that were within the bounds of acceptable accuracy.

Unfortunately, it was subsequently discovered that even the improved 9-point formulae failed to deliver the required accuracy for another type of extreme model (depicted in Fig. 1a), where there is a very sharp conductivity contrast (4000:1) at the Earth's surface.

In this paper we report our further investigations, which have led to an alternative formulation of the finite-difference equations that is numerically stable and yields quite accurate results for both types of extreme models shown in Figs 1(a) and (b). Two approaches are taken: in the first we calculate the field components at the nodes of the grid, as in P-A-W; in the second we use a staggered grid (Yee 1966), in which each component of the field has its own separate grid. Thus the standard solutions for the pair of models in Fig. 1, as given by a conventional finite-difference program, will be considered as a test package against which the results generated by any new formulation of the finite-difference equations must be tested. The program we used to generate the standard solutions was written by Poll (1994); it is based on the original scheme of Brewitt-Taylor & Weaver (1976) and Weaver & Brewitt-Taylor (1978), but includes several additional features and improvements such as integral boundary conditions on the Earth's surface and at the top of a uniform basement, and automatic grid generation. It has been used extensively in performing 2-D inversions (Agarwal, Poll & Weaver 1993).

2 FINITE-DIFFERENCE EQUATIONS FOR A FIXED GRID

In the usual notation (**E** for electric field, **B** for magnetic field, ρ for resistivity, vacuum permeability μ_0, and an $\exp(i\omega t)$ time dependence understood) the induction equations are

$$\operatorname{curl}\mathbf{E} = -i\omega\mathbf{B}, \qquad \rho\operatorname{curl}\mathbf{B} = \mu_0\mathbf{E}. \tag{1}$$

Given that all fields and model parameters are independent of the space variable x, the E-polarization components $\mathbf{E} = (U, 0, 0)$ and $\mathbf{B} = (0, Y, Z)$ satisfy the equations

$$U'(y,z) = -i\omega Y(y,z), \qquad \dot{U}(y,z) = i\omega Z(y,z),$$
$$\rho(y,z)[\dot{Z}(y,z) - Y'(y,z)] = \mu_0 U(y,z), \tag{2}$$

where $\dot{F} := \partial F/\partial y$ and $F' := \partial F/\partial z$ with F representing any of the electromagnetic components. Differentiating the third equation of (2) we obtain

$$-\frac{\partial}{\partial z}\{\rho(y,z)[\dot{Z}(y,z) - Y'(y,z)]\} = i\omega\mu_0 Y(y,z),$$

$$\frac{\partial}{\partial y}\{\rho(y,z)[\dot{Z}(y,z) - Y'(y,z)]\} = i\omega\mu_0 Z(y,z).$$

Since $\dot{Y} + Z' = 0$ (div $\mathbf{B} = 0$), we can augment these equations with vanishing terms as follows:

$$\frac{\partial}{\partial y}\{\rho(y,z)[\dot{Y}(y,z) + Z'(y,z)]\} - \frac{\partial}{\partial z}\{\rho(y,z)[\dot{Z}(y,z) - Y'(y,z)]\}$$
$$= i\omega\mu_0 Y(y,z), \tag{3}$$

$$\frac{\partial}{\partial z}\{\rho(y,z)[\dot{Y}(y,z) + Z'(y,z)]\} + \frac{\partial}{\partial y}\{\rho(y,z)[\dot{Z}(y,z) - Y'(y,z)]\}$$
$$= i\omega\mu_0 Z(y,z). \tag{4}$$

As we discovered in P-A-W, forms such as these are more

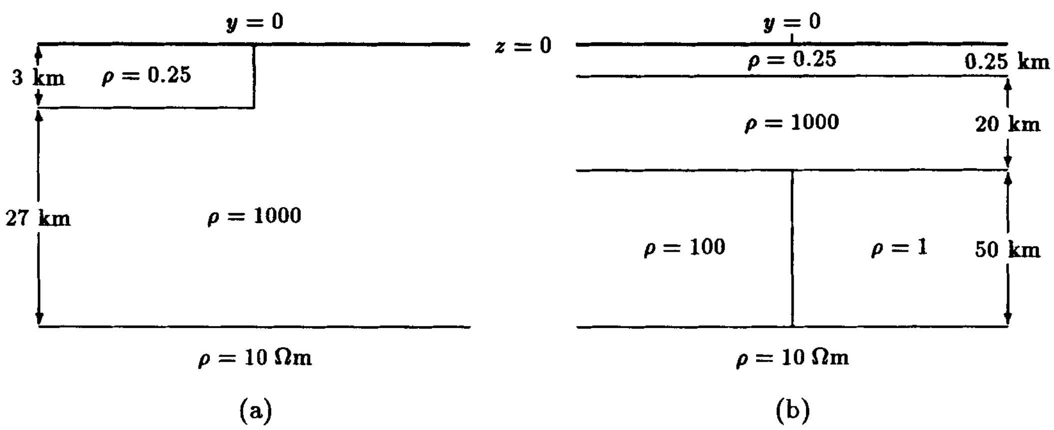

Figure 1. Two test models. The periods used in the calculations are 100 s for Model (a) and 1000 s for Model (b).

appropriate for integration since they lead to equations that are numerically stable.

In the model we let the conducting Earth occupy the region $z > 0$, with the half-space $z < 0$ representing the non-conducting atmosphere. The regional magnetic field is taken to be $Y_0\hat{\mathbf{y}}$. Vacuum permeability is assumed everywhere. A numerical grid covers the region $y_1 < y < y_M$, $z_1 < z < z_N$, where $z = z_1 = 0$ is the surface of the Earth, and $y = y_1$ and $y = y_M$, the side boundaries of the grid, are chosen to be sufficiently remote from the regions of anomalous resistivity that 1-D solutions (or asymptotic boundary conditions) are applicable there. The depth $D = z_N$ to which the grid extends is either the surface of a (1-D) layered half-space where an integal boundary condition can be applied, or is chosen to be sufficiently great that the field can be made vanishing there.

As in P-A-W, improved finite-difference equations are obtained by integrating around a typical node (m, n) at the grid point $y = y_m$, $z = z_n$. Here we label this node $(1, 1)$ for economy in writing, so that, for example, the neighbouring nodes $(m+1, n)$ and $(m, n-1)$ become $(2, 1)$ and $(1, 0)$, respectively. The node separations are h_0 and h_1 horizontally, and k_0 and k_1 vertically, as shown in Fig. 2. We define $h_+ = h_0 + h_1$ and $k_+ = k_0 + k_1$. Note that this notation differs slightly from that used in P-A-W.

Integrating eq. (3) over the rectangular domain whose vertices P, Q, R and S are at the centres of the four cells adjacent to the node $(1, 1)$, as shown in Fig. 2, and transforming the left-hand side by Green's theorem, we obtain

$$\left(\int_{\mathrm{SP}} + \int_{\mathrm{QR}}\right)\rho(\dot{Y} + Z')\,dz + \left(\int_{\mathrm{PQ}} + \int_{\mathrm{RS}}\right)\rho(\dot{Z} - Y')\,dy$$
$$= i\omega\mu_0 \iint_{\mathscr{A}} Y\,dy\,dz, \tag{5}$$

where $\mathscr{A}$ is the area of the rectangle PQRS. Note that we have already deviated from the procedure developed in P-A-W by including ρ in the first integrand while dispensing with dimensionless resistivities. A further variation is in the way we represent the derivatives in eq. (6) by central differences. Thus in the cell whose resistivity is $\rho_{3/2,3/2}$ (bottom right in Fig. 2)

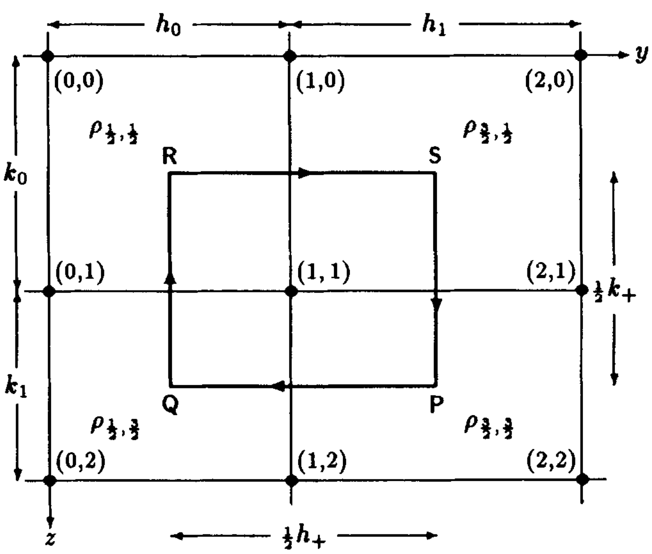

Figure 2. A typical node and the path of integration.

we now write (with F representing either Y or Z)

$$\dot{F} \approx \frac{F_{2,2} + F_{2,1} - F_{1,2} - F_{1,1}}{2h_1}, \quad F' \approx \frac{F_{2,2} + F_{1,2} - F_{2,1} - F_{1,1}}{2k_1}, \tag{6}$$

which are the averages of the central differences on the opposite sides of the cell. These expressions for the derivatives are used on that part of the contour of integration that lies within the cell, i.e. the lower section of SP and the right-hand section of PQ. Similar expressions hold in the other three cells. For points (y, z) within the domain of integration $\mathscr{A}$, we continue to set $F(y, z) \approx F_{1,1}$.

When these finite-difference approximations are substituted in (5), the resulting integrations are trivial and lead to the 9-point formula

$$\begin{aligned}(a_0 + i\omega\mu_0 h_+ k_+)Y_{1,1} &= a_1 Y_{2,1} + a_2 Y_{1,2} + a_3 Y_{0,1} + a_4 Y_{1,0}\\ &\quad + a_5 Y_{2,2} + a_6 Y_{0,2} + a_7 Y_{0,0} + a_8 Y_{2,0}\\ &\quad + b_1 Z_{2,1} + b_2 Z_{1,2} + b_3 Z_{0,1} + b_4 Z_{1,0},\end{aligned} \tag{7}$$

where

$$a_0 = \frac{h_+\rho_{1,3/2}}{k_1} + \frac{h_+\rho_{1,1/2}}{k_0} + \frac{k_+\rho_{3/2,1}}{h_1} + \frac{k_+\rho_{1/2,1}}{h_0},$$

$$a_1 = \frac{k_+\rho_{3/2,1}}{h_1} - \frac{h_1\rho_{3/2,3/2}}{k_1} - \frac{h_1\rho_{3/2,1/2}}{k_0},$$

$$a_2 = \frac{h_+\rho_{1,3/2}}{k_1} - \frac{k_1\rho_{3/2,3/2}}{h_1} - \frac{k_1\rho_{1/2,3/2}}{h_0},$$

$$a_3 = \frac{k_+\rho_{1/2,1}}{h_0} - \frac{h_0\rho_{1/2,3/2}}{k_1} - \frac{h_0\rho_{1/2,1/2}}{k_0},$$

$$a_4 = \frac{h_+\rho_{1,1/2}}{k_0} - \frac{k_0\rho_{3/2,1/2}}{h_1} - \frac{k_0\rho_{1/2,1/2}}{h_0},$$

$$a_5 = \left(\frac{h_1}{k_1} + \frac{k_1}{h_1}\right)\rho_{3/2,3/2}, \qquad a_6 = \left(\frac{h_0}{k_1} + \frac{k_1}{h_0}\right)\rho_{1/2,3/2},$$

$$a_7 = \left(\frac{h_0}{k_0} + \frac{k_0}{h_0}\right)\rho_{1/2,1/2}, \qquad a_8 = \left(\frac{h_1}{k_0} + \frac{k_0}{h_1}\right)\rho_{3/2,1/2},$$

$$b_1 = 2(\rho_{3/2,1/2} - \rho_{3/2,3/2}), \qquad b_2 = 2(\rho_{3/2,3/2} - \rho_{1/2,3/2}),$$

$$b_3 = 2(\rho_{1/2,3/2} - \rho_{1/2,1/2}), \qquad b_4 = 2(\rho_{1/2,1/2} - \rho_{3/2,1/2}).$$

Here we have defined the resistivities with subscript 1 to be the weighted average of the resistivity values in the relevant adjacent cells, for example

$$\rho_{1,1/2} = (h_1\rho_{3/2,1/2} + h_0\rho_{1/2,1/2})/h_+,$$

$$\rho_{3/2,1} = (k_1\rho_{3/2,3/2} + k_0\rho_{3/2,1/2})/k_+.$$

A similar treatment of eq. (4) gives

$$\begin{aligned}(a_0 + i\omega\mu_0 h_+ k_+)Z_{1,1} &= a_1 Z_{2,1} + a_2 Z_{1,2} + a_3 Z_{0,1} + a_4 Z_{1,0}\\ &\quad + a_5 Z_{2,2} + a_6 Z_{0,2} + a_7 Z_{0,0} + a_8 Z_{2,0}\\ &\quad - b_1 Y_{2,1} - b_2 Y_{1,2} - b_3 Y_{0,1} - b_4 Y_{1,0}.\end{aligned} \tag{8}$$

General formulae applicable at a mode (m, n) are readily obtained with the transformations $1 \to m$ or n as appropriate; $0 \to m-1$ or $n-1$; $2 \to m+1$ or $n+1$; $\frac{1}{2} \to m - \frac{1}{2}$ or $n - \frac{1}{2}$; $\frac{3}{2} \to m + \frac{1}{2}$ or $n + \frac{1}{2}$. It follows that $h_m := y_{m+1} - y_m$ and $k_n := z_{n+1} - z_n$, and we also note that $h_+ \to h_m^+ \equiv h_m + h_{m-1}$, $k_+ \to k_n^+ \equiv k_n + k_{n-1}$. There are $(M-2)(N-2)$ such pairs of equations, one for each node (m, n), $(m = 2, 3, \ldots, M-1;$ $n = 2, 3, \ldots, N-1)$. In our numerical experiments we have used sufficiently large grids that it can be assumed that the field values given by 1-D solutions are valid at the side nodes $(1, n)$ and (M, n), and that the field vanishes at the nodes (m, N) on the bottom of the grid. It remains, therefore, to state a pair of equations valid at each surface node $(m, 1)$.

One such equation is the same as that used by P-A-W, namely the Hilbert transform connecting the anomalous horizontal magnetic component with the vertical component, i.e.

$$Y(y, 0) - Y_0 = \frac{1}{\pi} \int_{-\infty}^{\infty} \frac{Z(u, 0)}{u - y}\, du. \tag{9}$$

Since Z vanishes in the 1-D regions of the model outside the domain of the grid, the integral evaluated at $y = y_m$ can be separated as follows:

$$Y_{m,1} - Y_0 = \frac{1}{\pi}\left[\int_{y_{m-1}}^{y_{m+1}} + \left(\sum_{p=1}^{m-2} + \sum_{p=m+1}^{M-1}\right)\int_{y_p}^{y_{p+1}}\right]\frac{Z(u, 0)}{u - y_m}\, du,$$

and then discretized by assuming that Z has a linear variation between the nodes. The resulting algebraic equation gives

$$Y_{m,1} = Y_0 + \frac{1}{\pi}\left[c_1^m Z_{1,1} + c_{m-1}^m Z_{m-1,1} + c_m^m Z_{m,1} + c_{m+1}^m Z_{m+1,1} + c_M^m Z_{M,1} + \left(\sum_{p=2}^{m-3} + \sum_{p=m+2}^{M-2}\right) c_p^m Z_{p,1}\right] \tag{10}$$

where, for $2 \le m \le M-1$,

$$c_m^m = \log(h_m/h_{m-1}),$$

$$c_p^m = \frac{y_{p+1} - y_m}{h_p}\log\left|1 + \frac{h_p}{y_p - y_m}\right| + \frac{y_m - y_{p-1}}{h_{p-1}}\log\left|1 + \frac{h_{p-1}}{y_{p-1} - y_m}\right|,$$

and for $3 \le m \le M-2$,

$$c_1^m = -1 - \frac{y_m - y_2}{h_1}\log\left(1 - \frac{h_1}{y_m - y_1}\right),$$

$$c_M^m = 1 - \frac{y_{M-1} - y_m}{h_{M-1}}\log\left(1 + \frac{h_{M-1}}{y_{M-1} - y_m}\right),$$

$$c_{m-1}^m = -(1 + h_{m-1}/h_{m-2})\log(1 + h_{m-2}/h_{m-1}),$$

$$c_{m+1}^m = (1 + h_m/h_{m+1})\log(1 + h_{m+1}/h_m),$$

with $c_1^2 = -1$ and $c_M^{M-1} = 1$. It is understood that the first sum in (10) disappears when $m = 2$ and the second when $m = M-1$.

For the other equation, P-A-W employed a Taylor expansion downwards from the surface. It gave perfectly reasonable results for the models considered by P-A-W, but we wonder whether this equation was one of the sources of trouble when calculations were made for models with high conductivity contrasts at the surface, such as the one shown in Fig. 1(a). Accordingly, we have replaced the second equation of P-A-W by a simple finite-difference representation of $\operatorname{div}\mathbf{B} = 0$ at the surface. Let $(1, 1)$ in Fig. 2 represent any node $(m, 2)$, $(m = 2, 3, \ldots, M-1)$ so that $(1, 0)$ corresponds to a surface node $(m, 1)$. In the two cells adjacent to $(m, 1)$, the finite-difference expressions (6) are used to express $\dot{Y} + Z' = 0$ in the form

$$\frac{Y_{m,1} - Y_{m-1,1} + Y_{m,2} - Y_{m-1,2}}{2h_{m-1}} + \frac{Z_{m,2} - Z_{m,1} + Z_{m-1,2} - Z_{m-1,1}}{2k_1} = 0,$$

$$\frac{Y_{m+1,1} - Y_{m,1} + Y_{m+1,2} - Y_{m,2}}{2h_m} + \frac{Z_{m,2} - Z_{m,1} + Z_{m+1,2} - Z_{m+1,1}}{2k_1} = 0.$$

In order not to introduce bias towards the cell on either the left or the right, we add the first of these equations multiplied by h_m to the second multiplied by h_{m-1} to obtain a finite-difference formula for $Z_{m,1}$ as follows:

$$Z_{m,1} = Z_{m,2} + \frac{h_m}{h_m^+}(Z_{m-1,2} - Z_{m-1,1}) + \frac{h_{m-1}}{h_m^+}(Z_{m+1,2} - Z_{m+1,1}) + \left(\frac{k_1}{h_{m-1}} - \frac{k_1}{h_m}\right)(Y_{m,1} + Y_{m,2}) + \frac{k_1}{h_m^+}\left[\frac{h_{m-1}}{h_m}(Y_{m+1,1} + Y_{m+1,2}) - \frac{h_m}{h_{m-1}}(Y_{m-1,1} + Y_{m-1,2})\right]. \tag{11}$$

Eqs (10) and (11) complete the linear system in the $2(M-2)(N-1)$ unknown values of the magnetic field components Y and Z at the interior and surface nodes of the grid. It is solved either by a direct method or by iteration.

In Figs 3 and 4 we have plotted the calculated values of the real and imaginary parts of the magnetic components Y and

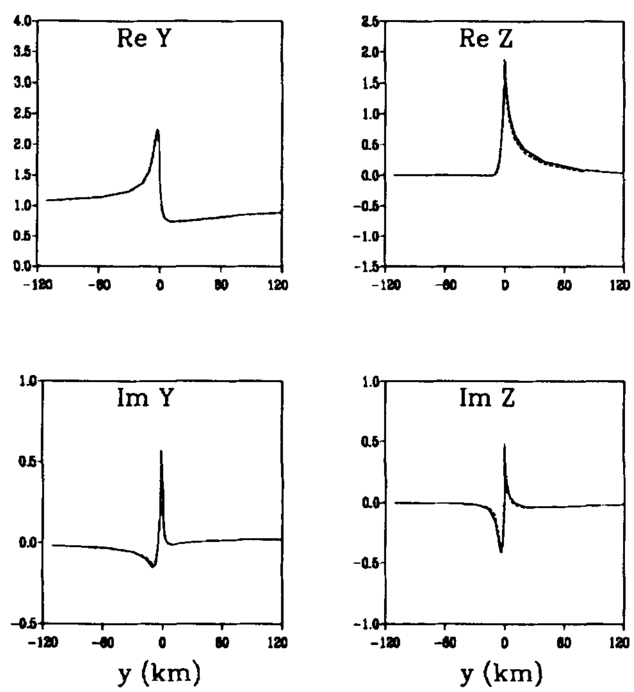

Figure 3. Real and imaginary parts of the magnetic field components Y and Z plotted along the surface $z = 0$ of the model shown in Fig. 1(a) for a period of 100 s. The field variations calculated directly in terms of Y and Z on a fixed grid are depicted by broken lines; the solid lines represent the same variations derived from the electric field obtained by the conventional finite-difference calculation.

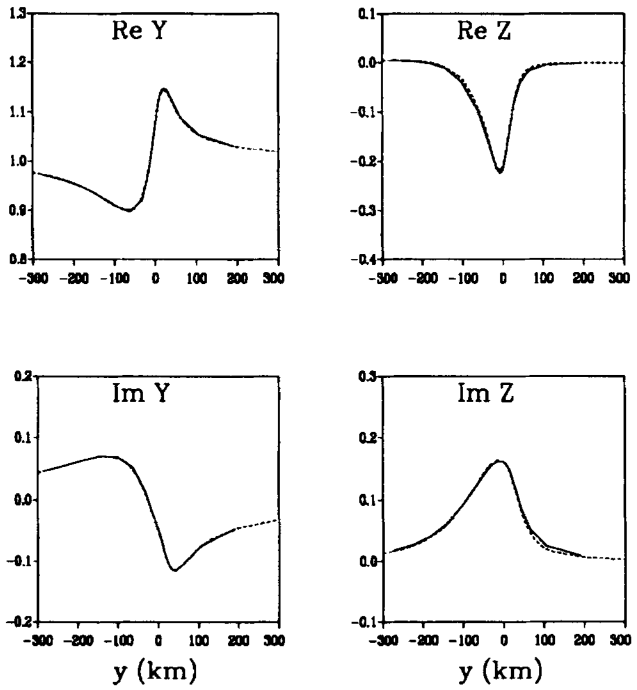

Figure 4. As Fig. 3, but for the test model shown in Fig. 1(b) and a period of 1000 s.

Z on the surface $z = 0$ at the respective periods of 100 and 1000 s for the two models shown in Figs 1(a) and (b). They are compared with the corresponding results obtained for the same models by the conventional finite-difference method in which the solution is obtained in terms of the electric field. It will be seen that there is such good agreement in all cases that the curves are barely distinguishable.

3 FINITE-DIFFERENCE EQUATIONS FOR A STAGGERED GRID

Staggered grids have only recently been employed in geo-electromagnetic numerical modelling (Wang & Hohmann 1993; Mackie, Madden & Wannamaker 1993; Mackie, Smith & Madden 1994), although they had already been used much earlier by Yee (1966) in the numerical solution of other problems in electromagnetism. They were also anticipated in the transmission surface and network analogies to electro-magnetic geophysical modelling discussed by Madden & Swift (1969) and Madden (1972). They are a particularly powerful tool in 3-D modelling because they automatically preserve the relations $\operatorname{div} \mathbf{B} = 0$ and $\operatorname{div}(\mathbf{E}/\rho) = 0$, as well as $\operatorname{curl} \mathbf{E} = 0$ when $\omega \to 0$. In two dimensions they offer no particular advantage in the conventional formulation of E- and B-polarization problems, but do provide an alternative approach to the solution of E-polarization problems in terms of the magnetic field, as we have been discussing here.

Fig. 5 shows how the various field components are defined on a staggered grid in relation to the four typical resistivity cells depicted in Fig. 2. The electric field into the plane of the diagram is defined at the centres of the cells, the horizontal magnetic field at the centre of each horizontal side of the cells, and the vertical magnetic components at the centre of each vertical side of the cells. This representation is equivalent to

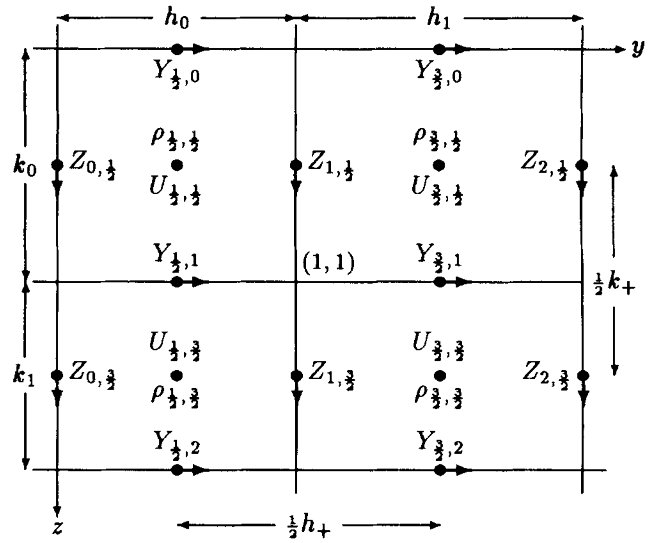

Figure 5. Field components defined on a staggered grid.

the (3-D) grid of Mackie *et al.* (1994), but differs from the one introduced by Yee (1966) in which the positions of the nodes for the electric and magnetic field components with respect to each resistivity cell were interchanged. Both approaches are possible in a 3-D setting, but the arrangement considered here is more convenient when solving E-polarization problems in two dimensions.

The finite-difference representation of the third induction equation of (2) at the node $(\frac{3}{2}, \frac{3}{2})$ is clearly

$$\mu_0 U_{3/2,3/2} = \rho_{3/2,3/2}\left(\frac{Z_{2,3/2} - Z_{1,3/2}}{h_1} - \frac{Y_{3/2,2} - Y_{3/2,1}}{k_1}\right). \tag{12}$$

The other equations in (2) are more difficult. One way of dealing with them is to return to the first equation of (1) from which they are derived, and to integrate it first over a rectangular domain perpendicular to the z-axis in Fig. 5, two of whose sides are parallel to the line joining the nodes $(\frac{1}{2}, \frac{3}{2})$ and $(\frac{3}{2}, \frac{3}{2})$, and the other two of which are of length 2ℓ divided at their midpoints by the plane of the diagram. Then an application of Stokes' theorem gives

$$\int_{-\ell}^{\ell} U_{1/2,3/2}\, dx + \int_{\ell}^{-\ell} U_{3/2,3/2}\, dx = -i\omega \iint_{\mathscr{S}} Z(y, z)\, dx\, dy, \tag{13}$$

where $\mathscr{S}$ is the area of the rectangle. As in Section 2, we set $Z(y, z) \approx Z_{1,3/2}$ for $(y, z) \in \mathscr{S}$, $U(y, z) \approx U_{1/2,3/2}$ in the lower left quadrant, and $U(y, z) \approx U_{3/2,3/2}$ in the lower right quadrant. It follows that the approximate form of (13) is

$$\frac{U_{3/2,3/2} - U_{1/2,3/2}}{h_+/2} = i\omega Z_{1,3/2}. \tag{14}$$

Similar arguments applied to an integration over a rectangular domain perpendicular to the y-axis yield

$$\frac{U_{3/2,3/2} - U_{3/2,1/2}}{k_+/2} = -i\omega Y_{3/2,1}. \tag{15}$$

Both of these equations will be recognized as rough finite-difference approximations of the first two equations of (2). If $h_0 = h_1$ and $k_0 = k_1$, they simplify to the standard central-difference formulae for first derivatives whose errors are $O(h^2)$ and $O(k^2)$, respectively. In general, however, formulae (14) and (15) have the larger errors $O(h)$ and $O(k)$. This can be seen by expanding a function $f(x)$ at a node 1 separated from node 0 by a distance d_0 and from node 2 by d_1, as follows:

$$f_2 = f_1 + d_1 f_1' + \frac{1}{2} d_1^2 f_1'' + O(d_1^2),$$

$$f_0 = f_1 - d_0 f_1' + \frac{1}{2} d_0^2 f_1'' + O(d_0^2).$$

Subtracting the second equation from the first we obtain

$$f_1' = \frac{f_2 - f_0}{d_0 + d_1} + \frac{1}{2}(d_0 - d_1) f_1'' + O(d^2), \tag{16}$$

or $f_1' \approx (f_2 - f_0)/(d_0 + d_1)$ which corresponds to (14) and (15). If $d_0 = d_1$, the error is $O(d^2)$ as noted earlier, but even in the general case the error is only weakly of order d because of the subtraction of the node separations. Incidentally, this error is no worse than that occurring in the standard 3-point finite-difference formula for the *second* derivative used in the standard finite-difference methods for solving the second-order differential equation satisfied by the electric field. In the finite-difference representation of the second derivative, the first term neglected is easily shown to be $(d_0 - d_1) f_1'''/3$ (Weaver 1994, p. 88), which is similar to the second term in (16) although the third derivative will probably be somewhat smaller than the second derivative appearing in (16).

Substititing (12) and the analogous equation at the node $(\frac{3}{2}, \frac{1}{2})$ in (15) and simplifying, we obtain

$$\left(\frac{\rho_{3/2,1/2}}{k_0} + \frac{\rho_{3/2,3/2}}{k_1} + \frac{1}{2} i\omega\mu_0 k_+\right) Y_{3/2,1}$$

$$= \frac{\rho_{3/2,1/2}}{k_0} Y_{3/2,0} + \frac{\rho_{3/2,3/2}}{k_1} Y_{3/2,2} + \frac{\rho_{3/2,1/2}}{h_1}(Z_{2,1/2} - Z_{1,1/2})$$

$$- \frac{\rho_{3/2,3/2}}{h_1}(Z_{2,3/2} - Z_{1,3/2}). \tag{17}$$

A similar substitution in (14) gives

$$\left(\frac{\rho_{1/2,3/2}}{h_0} + \frac{\rho_{3/2,3/2}}{h_1} + \frac{1}{2} i\omega\mu_0 h_+\right) Z_{1,3/2}$$

$$= \frac{\rho_{1/2,3/2}}{h_0} Z_{0,3/2} + \frac{\rho_{3/2,3/2}}{h_1} Z_{2,3/2} + \frac{\rho_{1/2,3/2}}{k_1}(Y_{1/2,2} - Y_{1/2,1})$$

$$- \frac{\rho_{3/2,3/2}}{k_1}(Y_{3/2,2} - Y_{3/2,1}). \tag{18}$$

Unfortunately, eqs (17) and (18) do not converge when an iterative solution is used. We attribute the non-convergence to round-off error generated, by the differences in field values on the right-hand side of (18) in regions of near lateral uniformity where Z is very small and Y scarcely varies horizontally. In fact, in a strictly 1-D model in which $\rho_{1/2,3/2} = \rho_{3/2,3/2}$ at all nodes, the pairs of horizontal field values $Y_{1/2,1}$ and $Y_{3/2,1}$, and $Y_{1/2,2}$ and $Y_{3/2,2}$, should exactly cancel out in (18) if Z is to be vanishing. Otherwise, a slightly non-vanishing numerical value for Z will be generated, which, in turn, will produce ever-increasing noise in (17) as the iteration proceeds, especially if $\rho_{3/2,1/2}$ or $\rho_{3/2,3/2}$ has a large value. The problem is avoided by transforming eq. (18) so that a difference in *resistivity* values ensures the exact vanishing of the critical terms. To do this we first note that elimination of U from (14), (15) and the corresponding equations associated with the nodes $(1, \frac{1}{2})$ and $(\frac{1}{2}, 1)$, respectively, verifies that

$$\frac{Y_{3/2,1} - Y_{1/2,1}}{h_+/2} + \frac{Z_{1,3/2} - Z_{1,1/2}}{k_+/2} = 0, \tag{19}$$

which is a finite-difference representation of div $\mathbf{B} = 0$ at (1, 1) expressed in terms of the less accurate finite-difference formulae for first derivatives discussed above. The analogous equation one cell-width below at (1, 2) is

$$\frac{Y_{3/2,2} - Y_{1/2,2}}{h_+/2} + \frac{Z_{1,5/2} - Z_{1,3/2}}{(k_1 + k_2)/2} = 0, \tag{20}$$

where the extension of the notation, with the introduction of k_2 and a subscript 5/2, into a cell lying beneath those shown in Fig. 5 is obvious. Eqs (19) and (20) can then be used to eliminate $Y_{1/2,1}$ and $Y_{1/2,2}$ respectively from (18). The resulting equation which replaces (18) is then

$$\left[\rho_{1/2,3/2}\left(\frac{1}{h_0} + \frac{h_+}{k_1(k_1 + k_2)} + \frac{h_+}{k_+ k_1}\right) + \frac{\rho_{3/2,3/2}}{h_1} + \frac{1}{2} i\omega\mu_0 h_+\right] Z_{1,3/2}$$

$$= \frac{\rho_{1/2,3/2}}{h_0} Z_{0,3/2} + \frac{\rho_{3/2,3/2}}{h_1} Z_{2,3/2} + \frac{h_+ \rho_{1/2,3/2}}{k_1}\left(\frac{Z_{1,1/2}}{k_+} + \frac{Z_{1,5/2}}{k_1 + k_2}\right)$$

$$+ \frac{\rho_{1/2,3/2} - \rho_{3/2,3/2}}{k_1}(Y_{3/2,2} - Y_{3/2,1}). \tag{21}$$

Even in regions of local uniformity in resistivity, the final term in (21) will automatically vanish when the neighbouring resistivities in the horizonal direction are equal. Eqs (17) and (21) are readily converted into forms applicable around a general interior point labelled (m, n), $(m = 2, 3, \ldots, M-1$; $n = 2, 3, \ldots, N-1)$, corresponding to (1, 1) shown in Fig. 5, by the transformations defined in Section 2.

A different treatment is required at the surface of the model earth, for, supposing that the nodes $(\frac{1}{2}, 1)$ and $(\frac{3}{2}, 1)$ in Fig. 5 are on the surface $z = 0$, we see that $Y_{3/2,0}$ in (17) and $Z_{1,1/2}$ in (21) represent field values above the earth, which is outside the domain of the numerical solution. Reverting to the general notation, we let $(m, 1)$ be a surface coordinate corresponding to (1, 1) in Fig. 5, and adjust the notation for the nodes on the staggered grid accordingly. For a modified version of eq. (21) which will be applicable at the node $(m, \frac{3}{2})$, we simply use eq. (20) by itself to eliminate $Y_{m-1/2,2}$ and leave $Y_{m-1/2,1}$ alone. Thus at $(m, \frac{3}{2})$ we have

$$\left[\rho_{m-1/2,3/2}\left(\frac{1}{h_{m-1}} + \frac{h_m^+}{k_1(k_1 + k_2)}\right) + \frac{\rho_{m+1/2,3/2}}{h_m} + \frac{1}{2} i\omega\mu_0 h_m^+\right] Z_{m,3/2}$$

$$= \frac{\rho_{m-1/2,3/2}}{h_{m-1}} Z_{m-1,3/2} + \frac{\rho_{m+1/2,3/2}}{h_m} Z_{m+1,3/2} + \frac{h_m^+ \rho_{m-1/2,3/2}}{k_1(k_1 + k_2)} Z_{m,5/2}$$

$$+ \frac{\rho_{m-1/2,3/2} - \rho_{m+1/2,3/2}}{k_1} Y_{m+1/2,2} + \frac{\rho_{m+1/2,3/2}}{k_1} Y_{m+1/2,1}$$

$$- \frac{\rho_{m-1/2,3/2}}{k_1} Y_{m-1/2,1}. \tag{22}$$

For the other surface equation we again use the Hilbert transform (9) with a modified discretization for its numerical evaluation. For $1 \le m \le M-1$ we write

$$Y_{m+1/2,1} - Y_0 = \frac{1}{\pi}\left[\fint_{y_m}^{y_{m+1}} + \left(\sum_{p=1}^{m-1} + \sum_{p=m+1}^{M-1}\right)\int_{y_p}^{y_{p+1}}\right] \times \frac{Z(u,0)}{u - y_{m+1/2}}\, du \qquad (23)$$

(with the understanding that the first sum vanishes when $m = 1$ and the second when $m = M - 1$), and assume that Z varies linearly between adjacent surface nodes. Thus, in the interval $y_m < y < y_{m+1}$ we let

$$Z(y, 0) = Z_{m,1} + (y - y_m)(Z_{m+1,1} - Z_{m,1})/h_m$$

and substitute in (23). The resulting integrations are quite straightforward and lead to a discrete equation of the form

$$Y_{m+1/2,1} = Y_0 + \frac{1}{\pi}\left[c_1 Z_{1,1} + c_m Z_{m,1} + c_{m+1} Z_{m+1,1} + c_M Z_{M,1} + \left(\sum_{p=2}^{m-1} + \sum_{p=m+2}^{M-1}\right) c_p Z_{p,1}\right], \qquad (24)$$

where, for $2 \le m \le M - 2$,

$$c_1 = -1 - \frac{y_{m+1/2} - y_2}{h_1}\log\left(1 - \frac{h_1}{y_{m+1/2} - y_1}\right),$$

$$c_M = 1 - \frac{y_{M-1} - y_{m+1/2}}{h_{M-1}}\log\left(1 + \frac{h_{M-1}}{y_{M-1} - y_{m+1/2}}\right),$$

$$c_m = -\left(1 + \frac{1}{2}h_m/h_{m-1}\right)\log(1 + 2h_{m-1}/h_m),$$

$$c_{m+1} = \left(1 + \frac{1}{2}h_m/h_{m+1}\right)\log(1 + 2h_{m+1}/h_m),$$

$$c_p = \frac{y_{m+1/2} - y_{p-1}}{h_{p-1}}\log\left|1 + \frac{h_{p-1}}{y_{p-1} - y_{m+1/2}}\right| + \frac{y_{p+1} - y_{m+1/2}}{h_p}\log\left|1 + \frac{h_p}{y_p - y_{m+1/2}}\right|,$$

again with the first sum in (24) vanishing when $m = 2$ and the second when $m = M - 2$.

Finally, it is necessary to relate the calculated values $Z_{m,3/2}$ in (22) to the corresponding surface values $Z_{m,1}$ in (24). There are several ways of doing this, all of them approximate. For example, a Taylor series expansion gives

$$Z_{m,3/2} = Z_{m,1} + \frac{1}{2}k_1 Z'_{m,1} + O(k_1^2) = Z_{m,1} - \frac{1}{2}k_1 \dot{Y}_{m,1} + O(k_1^2),$$

where we have used the fact that $\operatorname{div}\mathbf{B} = 0$. Expressing $\dot{Y}$ in the approximate finite-difference form that appeared in (19), and neglecting the terms $O(k_1^2)$, we obtain

$$Z_{m,1} = Z_{m,3/2} + (Y_{m+1/2,1} - Y_{m-1/2,1})k_1/h_m^+ . \qquad (25)$$

This equation, and its counterparts at $(m-1, 1)$ and $(m+1, 1)$, can be used to express $Z_{m-1,3/2}$, $Z_{m,3/2}$ and $Z_{m+1,3/2}$ appearing in (22), directly in terms of the surface values $Z_{m-1,1}$, $Z_{m,1}$ and $Z_{m+1,1}$ respectively. Alternatively, one could write $\operatorname{div}\mathbf{B}$ at the node $(m, \frac{3}{2})$ in the form

$$(Z_{m,2} - Z_{m,1})/k_1 + (Y_{m+1/2,1} + Y_{m+1/2,2} - Y_{m-1/2,1} - Y_{m-1/2,2})/h_m^+ ,$$

with $z_{m,2} = (k_1 Z_{m,5/2} + k_2 Z_{m,3/2})/k_2^+$, to obtain

$$Z_{m,1} = (k_1 Z_{m,5/2} + k_2 Z_{m,3/2})/k_2^+ + (k_1/h_m^+) \times (Y_{m-1/2,1} + Y_{m-1/2,2} - Y_{m+1/2,1} - Y_{m+1/2,2}). \qquad (26)$$

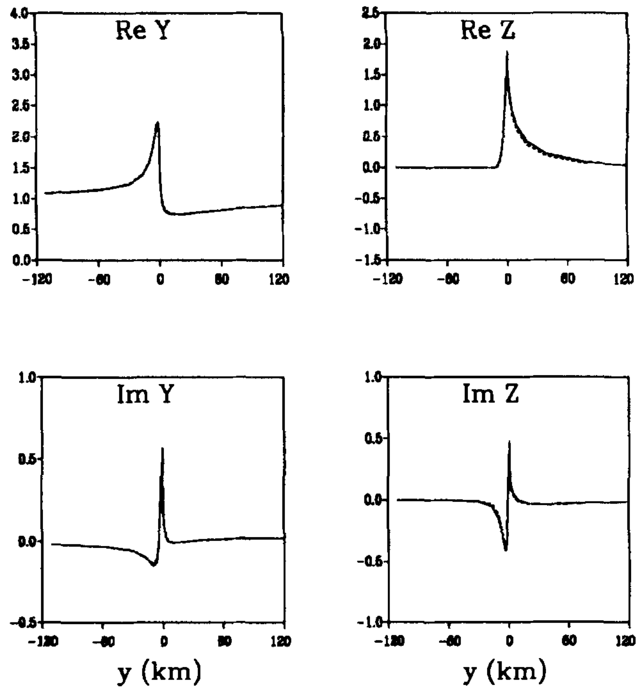

Figure 6. As Fig. 3, except that the broken lines now depict the field variations calculated on a staggered grid.

A third option is simply to express $Z_{m,3/2}$ as the average of $Z_{m,1}$ and $Z_{m,2}$, with $Z_{m,2}$ given by the weighted average defined above, whence

$$Z_{m,1} = (2 - k_2/k_2^+)Z_{m,3/2} - (k_1/k_2^+)Z_{m,5/2} . \qquad (27)$$

All three methods work quite well.

The system of equations defined by (17), (21), (22), (24) and (25) [or (26) or (27)], together with the boundary conditions specifying 1-D solutions for $Y_{3/2,n}$ and $Y_{M-1/2,n}$ and the vanishing of $Z_{1,n-1/2}$ and $Z_{M,n-1/2}$ ($n = 1, 2, \dots N$) on the sides of the grid, and also the vanishing of both $Y_{m+1/2,N}$ and $Z_{m,N-1/2}$ ($m = 1, 2, \dots M-1$) along its base, was found to converge when solved iteratively for all models on which the iteration scheme was tested, including those shown in Fig. 1. The values of the electric field at its own staggered grid points can then be found through an application of (12). The variations of the magnetic field components along the surface of the two models shown in Figs 1(a) and (b) calculated with the staggered grid are plotted in Figs 6 and 7 respectively, and are compared with the corresponding curves obtained by conventional finite-difference calculations. The agreement is as good as that observed in Figs 3 and 4, where the same field variations are calculated using a fixed grid.

4 THE SURFACE ELECTRIC FIELD

A simple numerical differentiation of the magnetic field components obtained on the fixed grid, followed by substitution in the third equation of (2), is not an effective way of computing the electric field at the Earth's surface. The horizontal derivative of the Z-component is discontinuous at a node between two regions of different resistivity, and there are difficulties associated with calculating the two one-sided derivatives at such a node with sufficient accuracy, while obtaining the vertical derivative (also one-sided) of Y at the Earth's surface also presents a problem. Moreover, if these two marginally accurate derivatives

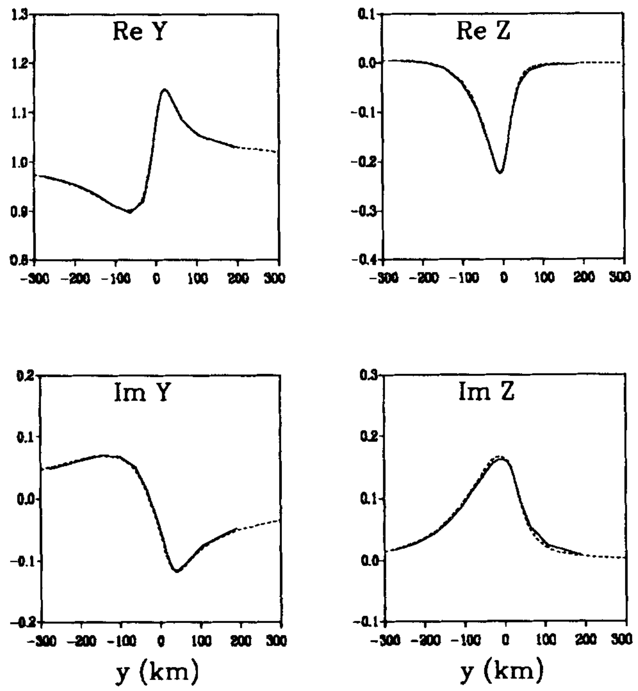

Figure 7. As Fig. 4, except that the broken lines now depict the field variations calculated on a staggered grid.

are of comparable magnitude, then the leading significant figures will be lost in the subtraction in (2), but the resulting inaccurate figure could then assume significance again through multiplication by the possibly very large factor ρ. In fact, the surface electric field calculated by this method for the model in Fig. 1(a) turned out to be both inaccurate and erratic in behaviour.

Our preferred method is to use the integral form of the first equation of (1). Consider a rectangular contour of width 2ℓ in the x-direction and extending vertically from the surface $z=0$ down to the base of the grid at $z=D$. Integrating the first equation of (1) over the area enclosed by the contour and applying Stokes' theorem, we obtain

$$\int_{\ell}^{-\ell} U(y,0)\,dx + \int_{-\ell}^{\ell} U(y,D)\,dx = -i\omega \int_{-\ell}^{\ell}\int_{0}^{D} Y(y,z)\,dz\,dx\,.$$

The factors 2ℓ which arise from the integrations over x cancel out, leaving an equation which, at $y=y_m$, takes the form

$$U_{m,1} = U_{m,N} + i\omega \int_0^D Y(y_m, z)\,dz\,. \tag{28}$$

The integral on the right-hand side can be discretized in the usual way by assuming a linear variation of the field between nodes, whence

$$U_{m,1} = U_{m,N} + \frac{1}{2} i\omega \left(k_1 Y_{m,1} + k_{N-1} Y_{m,N} + \sum_{p=2}^{N-1} k_p^+ Y_{m,p} \right). \tag{29}$$

If, as we have assumed in the previous sections, the depth D to which the grid extends is taken to be large enough that both U and Y are vanishingly small at the nodes (m, N), then (29) simplifies to

$$U_{m,1} = \frac{1}{2} i\omega \left(k_1 Y_{m,1} + \sum_{p=2}^{N-1} k_p^+ Y_{m,p} \right). \tag{30}$$

Otherwise an integral boundary condition must be used to express $U_{m,N}$ in terms of $Y_{m,N}$. For example, if $z=D$ is the surface of a basement half-space of uniform conductivity σ and skin depth $\delta \equiv (2/\omega\mu_0\sigma)^{1/2}$, then

$$U_{m,N} = \frac{i\omega}{\pi} \int_{-\infty}^{\infty} Y(y_m, D) K_0[(1+i)|y_m - v|/\delta]\,dv$$

(Weaver 1994, p. 117), where K_0 is the modified Bessel function of the second kind. In our numerical experiments, eq. (30) was used to calculate the electric field at the surface nodes from the values of Y calculated by the method described in Section 2.

On the staggered grid, values of the electric field U are calculated at grid points $(m+\frac{1}{2}, \frac{3}{2})$, $(m=2, 3, \ldots, M-2)$, one half of a cell-thickness beneath the surface. They can be related to surface values at the same nodes $(m+\frac{1}{2}, 1)$ as those where the horizontal magnetic field component Y is defined, by a similar integration to that described above except that this time the rectangular contour extends only to the depth $k_1/2$. The resulting equation corresponding to (28) is

$$U_{m+1/2,1} = U_{m+1/2,3/2} + i\omega \int_0^{k_1/2} Y(y_{m+1/2}, z)\,dz\,,$$

which is integrated with the usual assumption that Y varies linearly between nodes, to yield

$$U_{m+1/2,1} = U_{m+1/2,3/2} + \frac{1}{8} i\omega (3Y_{m+1/2,1} + Y_{m+1/2,2})\,. \tag{31}$$

The variations of the electric field along the surface $z=0$ calculated on both fixed and staggered grids [eqs (30) and

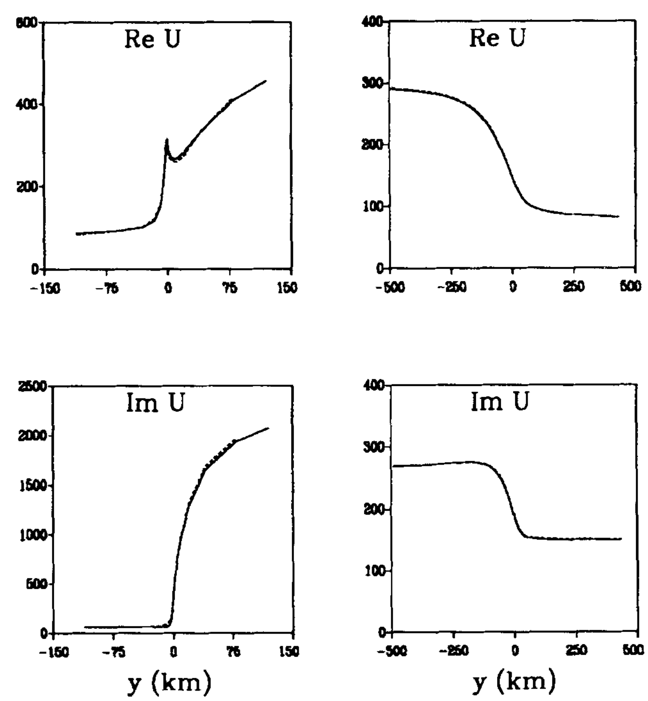

Figure 8. Real and imaginary parts of the electric field component U plotted along the surface $z=0$ of the models shown in Fig. 1(a) for a period of 100 s (left-hand column), and in Fig. 1(b) for a period of 1000 s (right-hand column). Calculations performed on the fixed grid according to eqn. (30) are depicted by the broken lines. The solid lines represent the same variations computed directly using the conventional finite-difference program.

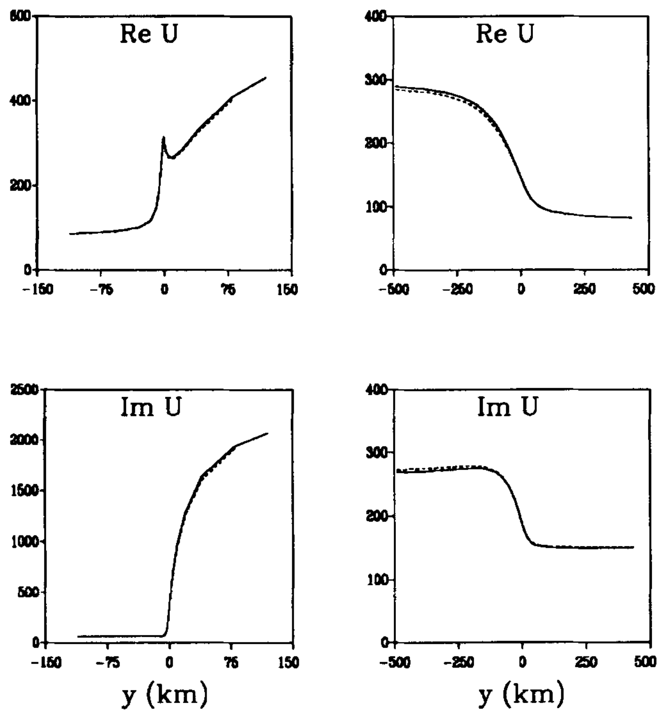

Figure 9. As Fig. 8 except that the broken lines now represent the field variations computed according to eq. (31) on a staggered grid.

(31) respectively] are compared in Figs 8 and 9 with those obtained directly using a standard finite-difference program for the two test models shown in Fig. 1. The agreement is again found to be excellent.

5 CONCLUDING REMARKS

What at first sight appears to be a straightforward problem—solving directly for the magnetic field in 2-D modelling of E-polarization induction—has turned out to be one fraught with numerical difficulties. In a previous paper we dealt with the problem of achieving computational accuracy for a certain class of models and ensuring numerical stability in the application of improved 9-point finite-difference formulae. Here we have turned our attention to maintaining numerical accuracy and stability even for models with extreme conductivity contrasts. We have even performed calculations similar to those presented in this paper for a model with a surface conductivity contrast of 40 000 : 1 with no loss of accuracy. Several modifications to the 9-point finite-difference formulae developed for a fixed grid in the previous paper have been proposed, and an alternative scheme designed for application with a staggered grid has also been investigated. Both methods give very accurate results. On balance, the staggered-grid formulae are somewhat simpler to obtain and more robust in application. It is interesting to note, for example, that whereas the finite-difference representation of the third equation of (2) was used to compute the electric field without difficulty in the staggered-grid formulation, it failed to provide accurate results on the fixed grid when the conductivity contrast was high; staggered grids certainly appear to be ideally suited to the finite-difference representation of electromagnetic fields. On the other hand, fixed grids are convenient when determining values of apparent resistivity, phase, and induction vector magnitudes because all of the magnetic and electric field components are then calculated at the same nodes, and, unlike the staggered grid points, such nodes are always located at conductivity boundaries on the surface of the Earth, which are critical points in defining the behaviour of the field variations. We have demonstrated that it is possible, with appropriately chosen finite-difference formulae, to compute the magnetic field components for models with high conductivity contrasts to the same degree of accuracy as obtained with staggered grids, and a method of calculating the associated electric field which avoids numerical differentiation has also been derived.

The information gleaned from this investigation is primarily of interest in 3-D modelling, not only because such 2-D problems arise quite naturally on the sides of a 3-D grid, but also because the methods developed here provide pointers on how to handle the corresponding numerical difficulties in full-scale 3-D modelling. In particular, provided that the condition $\operatorname{div} \mathbf{B} = 0$ is explicitly or implicitly included in the finite-difference equations, the evidence suggests that it is possible to generate numerically accurate and stable solutions on a fixed grid even for models with high conductivity contrasts, notwithstanding the assertion sometimes made that staggered grids are essential in 3-D modelling. A preliminary report on this topic has been presented by Weaver, Agarwal & Pu (1995), and will be discussed in more detail in a future paper.

ACKNOWLEDGMENTS

This work was supported by grants from the Natural Sciences and Engineering Research Council of Canada and the University of Victoria.

REFERENCES

Agarwal, A.K., Poll, H.E. & Weaver, J.T., 1993. One- and two-dimensional inversion of magnetotelluric data in continental regions, *Phys. Earth planet. Inter.*, **81**, 155–176.

Brewitt-Taylor, C.R. & Weaver, J.T., 1976. On the finite difference solution of two-dimensional induction problems, *Geophys. J. R. astr. Soc.*, **47**, 375–396.

Mackie, R.L., Madden, T.R. & Wannamaker, P.E., 1993. Three-dimensional magnetotelluric modeling using difference equations—Theory and comparisons to integral equation solutions, *Geophysics*, **58**, 215–226.

Mackie, R.L., Smith, J.T. & Madden, T.R., 1994. Three-dimensional electromagnetic modeling using finite difference equations: The magnetotelluric example, *Radio Science*, **29**, 923–935.

Madden, T.R., 1972. Transmission systems and network analogies to geophysical forward and inverse problems, *ONR Tech. Rep.*, 72–73.

Madden, T.R. & Swift, C.M., 1969. Magnetotelluric studies of the electrical conductivity structure of the crust and upper mantle, in *The Earth's Crust and Upper Mantle*, ed. Hart, P.J., AGU Monograph **13**, 469–479.

Poll, H.E., 1994. Automatic Forward Modelling of Two-Dimensional Problems in Electromagnetic Induction, *PhD thesis*, University of Victoria, BC, Canada.

Pu, X.H., Agarwal, A.K. & Weaver, J.T., 1993. Magnetic field solutions of E-polarization induction problems, *J. Geomag. Geoelectr.*, **45**, 859–872. (P-A-W)

Wang, T. & Hohmann, G.W., 1993. A finite-difference time-domain solution for three-dimensional electromagnetic modeling, *Geophysics*, **58**, 797–809.

Weaver, J.T., 1994. *Mathematical Methods for Geo-electromagnetic Induction*, Research Studies Press, Taunton, UK.

Weaver, J.T. & Brewitt-Taylor, C.R., 1978. Improved boundary conditions for the numerical solution of E-polarization problems in geomagnetic induction, *Geophys. J. R. astr. Soc.*, **54,** 309–317.

Weaver, J.T., Agarwal, A.K. & Pu, X.H., 1995. Recent developments in three-dimensional finite difference modelling of the magnetic field in geo-electromagnetic induction, in *Three-Dimensional Electromagnetics* pp. 131–141, eds Oristaglio, M.L. & Spies, B.R., International Symposium Abstracts, Schlumberger-Doll Res., Ridgefield, CT.

Yee, K.S., 1966. Numerical solution of initial boundary value problems involving Maxwell's equations in isotropic media, *IEEE Trans.*, **AP-14,** 302–307.